ISSN 1070-3284, Russian Journal of Coordination Chemistry, 2017, Vol. 43, No. 4, pp. 223–231. © Pleiades Publishing, Ltd., 2017.
Original Russian Text © E.V. Korneeva, A.-C. Larsson, A.V. Ivanov, E.V. Novikova, A.I. Smolentsev, O.N. Antzutkin, 2017, published in Koordinatsionnaya Khimiya, 2017, Vol. 43, No. 4, pp. 230–237.

Crystalline Nickel(II) Di-*i*-Amyl Dithiophosphate, $[Ni\{S_2P(O\text{-}i\text{-}C_5H_{11})_2\}_2]$: Preparation, Structure, Heteronuclear (^{13}C, ^{31}P) CP/MAS NMR Spectra, and Thermal Behavior

E. V. Korneeva[a], A.-C. Larsson[b], A. V. Ivanov[a, *], E. V. Novikova[a], A. I. Smolentsev[c, d], and O. N. Antzutkin[b]

[a] *Institute of Geology and Nature Management, Far East Branch, Russian Academy of Sciences, Blagoveshchensk, 675000 Russia*
[b] *Chemistry of Interfaces, Luleå University of Technology, S-971 87, Luleå, Sweden*
[c] *Nikolaev Institute of Inorganic Chemistry, Siberian Branch, Russian Academy of Sciences, Novosibirsk, 630090 Russia*
[d] *Novosibirsk State University, Novosibirsk, 630090 Russia*
**e-mail: alexander.v.ivanov@chemist.com*

Received June 14, 2016

Abstract—The crystalline nickel(II) di-*i*-amyl) dithiophosphate (Dtph), $[Ni\{S_2P(O\text{-}i\text{-}C_5H_{11})_2\}_2]$ (**I**) was isolated on a preparative scale and characterized by ^{13}C, ^{31}P MAS NMR, and X-ray diffraction (CIF file CCDC no. 1469369). The χ^2-statistic diagrams were constructed from full ^{31}P CP/MAS NMR spectra for calculating the ^{31}P chemical shift anisotropy: $\delta_{aniso} = \delta_{zz} - \delta_{iso}$ and the asymmetry parameter $\eta = (\delta_{yy} - \delta_{xx})/(\delta_{zz} - \delta_{iso})$. The key structural unit of **I** is the centrosymmetric $[Ni\{S_2P(O\text{-}i\text{-}C_5H_{11})_2\}_2]$ molecule in which the nickel atom coordinates two Dtph ligands in the isobidentate fashion. In molecule **I**, each carbon, oxygen, and sulfur atom is statistically disordered over two sites with equal occupancies. However, the disorder does not affect nickel and phosphorus. These results were interpreted as the presence in **I** of two $[Ni\{S_2P(O\text{-}i\text{-}C_5H_{11})_2\}_2]$ molecules rotated through 21.0(1)° (the angle between the $[NiS_4]$ chromophore planes) relative to each other around the bisecting P–Ni–P axis passing through both four-membered $[NiS_2P]$ rings. The two molecules occupy crystal lattice sites with equal probabilities. The thermal behavior of **I** was studied by simultaneous thermal analysis under argon. The course of the thermal destruction of the complex was established, nickel pyrophosphate ($Ni_2P_2O_7$) was identified as the final product of thermal transformations.

Keywords: nickel(II) dialkyl dithiophosphate complexes, molecular structures, structural disorder, ^{13}C and ^{31}P CP/MAS NMR spectroscopy, ^{31}P chemical shift anisotropy, thermal transformations of nickel(II) dithiophosphates

DOI: 10.1134/S1070328417040030

INTRODUCTION

Dialkyl dithiophosphoric acids are widely used in analytical chemistry (in extraction and complexation and in the instrumental determination of metals). Ionic *O*,*O*'-dialkyl dithiophosphates, which are the major components of commercial Aerofloat and Danafloat formulations, are also significant for flotation enrichment of non-ferrous metal ores and as selective reagent collectors required for effective separation of sulfide minerals of various chemical nature under the froth flotation. Transition metal dialkyl dithiophosphate complexes also find wide use as engine and lubricating oil additives and effective antioxidants for polyolefins. A number of crystalline dialkyl and diaryl dithiophosphates $[Ni\{S_2P(OR)_2\}_2]$ have now been structurally characterized (R = CH_3 [1], C_2H_5 [2–4], C_3H_7 [5], *i*-C_3H_7 [6], *i*-C_4H_9 [5, 7], *sec*-C_4H_9 [7], *cyclo*-C_5H_9 [8], *cyclo*-C_6H_{11} [9, 10], $CH_2C_6H_5$ [11], $CH_2CH_2C_6H_5$ [12], *o*-CH_3-C_6H_4, *m*-CH_3-C_6H_4 [10], and *p*-*tert*-C_4H_9-C_6H_4 [13]). Nickel(II) complexes with optically active dithiophosphate ligands, in which cyclic substituents contain chiral carbon atoms, have also been studied [14, 15] (R_2 = $CH(CH_3)$–$CH(CH_3)$ [14], R = 2-*i*-C_3H_7-5-CH_3-*cyclo*-C_6H_9 [15]); the structures of various isomeric forms (two enantiomers and the *meso*-form) have been considered.

Furthermore, nickel(II) complexes in which the dithiophosphate ligands occur in the outer sphere and are held by hydrogen bonds are known [16]. The catalytic activity of $[Ni\{S_2P(OCH_2CH_2C_6H_5)_2\}_2]$ towards the hydrolysis of carboxylic acid esters has been studied in [12]. The crystal structure of nickel(II) dipropyl dithiophosphate was found to comprise alternating isomeric centrosymmetric $[Ni\{S_2P(OC_3H_7)_2\}_2]$ molecules [5]. Depending on the preparation conditions,

the di-*iso*-butyl dithiophosphate complex exists as two forms, α- [5] and β- [7] ones, one consisting of noncentrosymmetric and the other consisting of centrosymmetric $[Ni\{S_2P(O\text{-}i\text{-}C_4H_9)_2\}_2]$ molecules. It was found that with temperature rise, the non-centrosymmetric α-form molecules are transformed into centrosymmetric ones; the equilibrium between the two forms exists up to complete transition of the sample to the β-form at 323 K. However, the structures of nickel(II) dithiophosphate complexes comprising long-chain alkyl groups remain unexplored because even nickel(II) *O*,*O*'-dibutyl dithiophosphate is a liquid (dark violet-colored) [5], like the corresponding platinum(II) complexes [17].

As a continuation of the mentioned studies, here we prepared the crystalline nickel(II) *O*,*O*'-di-*i*-amyl dithiophosphate, $[Ni\{S_2P(O\text{-}i\text{-}C_5H_{11})_2\}_2]$ (**I**), and studied its monomeric planar tetragonal structure, including the disordered carbon, oxygen, and sulfur atoms, by X-ray diffraction and ^{13}C and ^{31}P CP/MAS NMR; in particular, refined parameters of the ^{31}P chemical shift anisotropy, δ_{aniso} and η, were determined. A simultaneous thermal analysis (STA) study of I demonstrated that thermal decomposition occurs formally in one step with subsequent smooth desorption of thermolysis products. The final product of thermal transformations is nickel(II) pyrophosphate, $Ni_2P_2O_7$.

EXPERIMENTAL

Synthesis. A cooled solution of $K\{S_2P(O\text{-}i\text{-}C_5H_{11})_2\}$ (CHEMINOVA AGRO A/S, Denmark) (0.103 g, 0.3338 mmol) in 10 mL of water was added with stirring to a solution containing $NiSO_4 \cdot 7H_2O$ (0.047 g, 0.1673 mmol) in 20 mL of water cooled to 0°C. The resulting whitish-violet emulsion (with traces of violet oil on the surface) was left overnight in a refrigerator. The dark violet bulky precipitate thus formed was collected on a filter, washed with water, and dried on the filter at room temperature (84% yield). The transparent violet crystals of **I** for X-ray diffraction were obtained from ethanol at −12°C. $K\{S_2P(O\text{-}i\text{-}C_5H_{11})_2\}$ used in the synthesis was additionally characterized by ^{13}C CP/MAS NMR (δ, ppm):

$K\{S_2P(O\text{-}i\text{-}C_5H_{11})_2\}$: (1 : 1 : 1 : 2) 66.6 ($-OCH_2-$); 41.0; 39.1 (1 : 1, $-CH_2-$); 26.7; 26.4 (1 : 1, $-CH=$); 25.0; 23.9; 23.6; 22.9; 22.7 ($-CH_3$) [5].

The $^{13}C/^{31}P$ CP/MAS NMR spectra were measured on a Fourier Transform pulsed CMX-360 spectrometer (Varian/Chemagnetics InfinityPlus) operating at 90.52/145.71 MHz with a superconducting magnet (B_0 = 8.46 T). The spectra were recorded with cross-polarization from protons and $^{13}C-^{1}H/^{31}P-^{1}H$ decoupling using the radiofrequency field at the proton resonance frequency [18]. A ~40 mg sample was placed into a ceramic (ZrO_2) rotor 4.0 mm in diameter. The magic angle spinning was performed at 3000–6300/1600–3700(1) Hz; 64/4 acquisitions; proton π/2 pulses of 3.3–5.0/3.3 μs duration; $^{1}H-^{13}C/^{1}H-^{31}P$ contact time of 2.2–2.5/2.5 ms; and 2.0–3.0/5.0 s delay between the excitation pulses. The isotropic ^{13}C chemical shifts are given in ppm and referred to one component of external crystalline adamantane [19] (δ = 38.48 ppm relative to tetramethylsilane) [20]) and the ^{31}P chemical shifts were referred to 85% H_3PO_4 [21]. The magnetic field homogeneity was monitored by considering the width of the adamantane reference line of 2.6 Hz. The isotropic chemical shifts were corrected for the magnetic field strength drift, whose frequency equivalent was 0.051/0.110 Hz/h for the $^{13}C/^{31}P$ nuclei. The ^{31}P chemical shift anisotropy, $\delta_{aniso} = \delta_{zz} - \delta_{iso}$, and the asymmetry parameter of the ^{31}P chemical shift tensor, $\eta = (\delta_{yy} - \delta_{xx})/(\delta_{zz} - \delta_{iso})$, were derived from χ^2-statistics [22]. They were based on analysis of the sideband integral intensity ratios [23, 24] in full ^{31}P CP/MAS NMR spectra recorded at two sample spinning frequencies: 3700(1) and 1600(1) Hz. The calculations were performed using the Mathematica program [25].

X-ray diffraction. A cubic single crystal of **I** was attached to the tip of a glass capillary by epoxy resin. The experiment was carried out on a Bruker-Nonius X8 Apex CCD diffractometer (MoK_α radiation, λ = 0.71073 Å, graphite monochromator) at 150(2) K. The data were collected by a standard procedure: φ scanning of narrow frames. The absorption corrections were applied empirically using the SADABS program [26]. The structure was solved by the direct method and refined by least squares (on F^2) in the full-matrix anisotropic approximation of non-hydrogen atoms. All carbon, oxygen, and sulfur atoms are randomly distributed between two positions with equal occupancies (0.5). The hydrogen positions for the dithiophosphate ligands were calculated geometrically and included in the refinement in the riding model. The structure determination and refinement calculations were carried out using the SHELXTL program package [26]. The key crystallographic data and structure refinement details for **I** are summarized in Table 1 and selected bond lengths and angles are given in Table 2.

The atom coordinates, bond lengths, and bond angles are deposited with the Cambridge Crystallographic Data Centre (no. 1469369; deposit@ccdc.cam.ac.uk or http://www.ccdc.cam.ac.uk).

The thermal behavior of **I** was studied by STA with simultaneous recording of thermogravimetry (TG) and differential scanning calorimetry (DSC) curves. The measurements were carried out on a STA 449C Jupiter (NETZSCH) instrument in corundum crucibles covered with a lid with a hole to ensure a pressure of 1 atm during the thermal decomposition of the sample. Heating was performed under argon at a rate

Table 1. Crystallographic data and experimental and structure refinement details for **I**

Parameter	Value
Molecular formula	$C_{20}H_{44}O_4S_4P_2Ni$
M	597.44
System	Cubic
Space group	$Im\overline{3}$
a, Å	16.743(2)
V, Å^3	4693.5(10)
Z	6
ρ(calcd.), g/cm^3	1.268
μ, mm^{-1}	1.011
F(000)	1908
Crystal size, mm	0.36 × 0.34 × 0.25
θ Range for data collection, deg	1.72–25.65
Reflection index ranges	$-11 \le h \le 11$, $-20 \le k \le 8$, $-20 \le l \le 6$
Reflections collected	2869
Independent reflections (R_{int})	809 (0.0288)
Reflections with $I > 2\sigma(I)$	477
Refinement parameters	73
GOOF	1.064
R-factors for $F^2 > 2\sigma(F^2)$	$R_1 = 0.0670$, $wR_2 = 0.1984$
R-factors for all reflections	$R_1 = 0.1063$, $wR_2 = 0.2206$
Residual electron density (max/min), e/Å^3	0.714/–0.209

Table 2. Selected bond lengths (d) and bond angles (ω) in structure **I***

Bond	d, Å	Bond	d, Å
Ni(1)–S(1)	2.213(3)	C(1)–C(2)	1.53(2)
S(1)–P(1)	1.960(4)	C(2)–C(3)	1.47(2)
P(1)–O(1)	1.602(7)	C(3)–C(4)	1.54(2)
C(1)–O(1)	1.468(12)	C(3)–C(5)	1.59(2)
Angle	**ω, deg**	**Angle**	**ω, deg**
S(1)Ni(1)S(1)^a	87.9(2)	C(1)O(1)P(1)	118.0(7)
S(1)Ni(1)S(1)^b	92.1(2)	O(1)C(1)C(2)	107.5(10)
Ni(1)S(1)P(1)	84.47(14)	C(1)C(2)C(3)	115.6(13)
S(1)P(1)S(1)^a	103.2(2)	C(2)C(3)C(4)	115.2(12)
S(1)P(1)O(1)	119.0(3)	C(2)C(3)C(5)	108.3(12)
S(1)^{a}P(1)O(1)	106.9(3)	C(4)C(3)C(5)	102.0(12)
O(1)P(1)O(1)^a	102.8(6)		

* Symmetry codes: ^{a} $1 - x, y, -z$; ^{b} $x, 1 - y, z$.

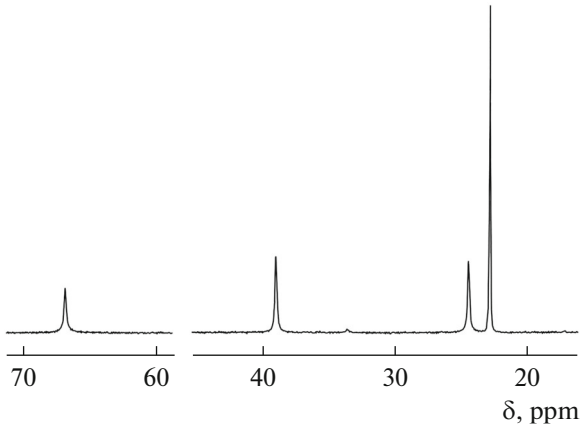

Fig. 1. ^{13}C CP/MAS NMR spectrum of compound **I**; number of acquisitions/spinning frequency: 680/6.3 kHz.

of 5 K/min up to 1100°C. For clearer identification of the thermal effects in the initial stage, the measurements were additionally performed in aluminum crucibles. The sample weight was 3.675–7.105 mg. The accuracy of temperature measurement was ±0.7°C, and the weight variation was $\pm 1 \times 10^{-4}$ mg. The TG and DSC curves were recorded using a correction file and temperature and sensitivity calibrations for the specified temperature program and heating rate. The melting point of **I** was also measured on a PTP(M) instrument (JSC Khimlaborpribor).

High-resolution scanning electron microscopy was used to study the degree of dispersion and morphology of **I** and the products formed in various thermal decomposition stages (a JSM 6390LV JEOL scanning electronic microscope equipped with an Oxford INCA Energy 350-Wave microanalysis system with energy and wavelength dispersion). The chemical composition was determined qualitatively by microprobe technique using an energy-dispersive spectrometer. The measurements were carried out at the Analytical Center of the Institute of Geology and Nature Management (Far East Branch of the Russian Academy of Sciences).

The IR spectra of the final residue formed upon thermolysis of **I** were recorded in KBr pellets on an FSM–1201 (Infraspek) interference FT IR spectrometer in the 400–4000 cm^{-1} range with a resolution of 1.0 cm^{-1} and 20 acquisitions. The spectra were treated using the FSpec program (version 4.0.0.2 for Windows, LLC Monitoring).

RESULTS AND DISCUSSION

The unusually simple ^{13}C CP/MAS NMR spectrum of crystalline complex **I** (Fig. 1) shows the $-OCH_2-$ (66.9), $-CH_2-$ (39.1), $-CH=$ (24.6), and $-CH_3$ (23.0 ppm) groups of the four alkoxy substituents of the dithiophosphate (Dtph) ligands as single resonance singlets (1 : 1 : 1 : 2), which is indicative of the intra- and interligand equivalence of the structural sites of the corresponding carbon atoms and a high degree of symmetry of the $[Ni\{S_2P(O\text{-}i\text{-}C_5H_{11})_2\}_2]$ molecule. In turn, the only resonance signal at the center of gravity of the full ^{31}P CP/MAS NMR spectrum with an isotropic ^{31}P chemical shift reflects the structural equivalence of the Dtph ligands (Fig. 2). The isotropic ^{31}P chemical shift of the di-*i*-amyl dithiophosphate ligands in complex I is much smaller (δ_{iso} = 95.0 ppm) than that in the initial salt $K\{S_2P(O\text{-}i\text{-}C_5H_{11})_2\}$, which is mainly ionic (δ_{iso} = 108.8 ppm). The increasing degree of electron shielding of the ^{31}P nucleus is a direct consequence of covalent binding of Dtph to nickel(II). The full ^{31}P CP/MAS NMR spectral pattern of compound **I** attests to a nearly axial symmetry of the ^{31}P chemical shift tensor (Figs. 2a, 2b). For gaining quantitative data on the ^{31}P chemical shift anisotropy and establishing the structural function of the Dtph groups in **I**, χ^2-statistic diagrams (Fig. 3) were constructed as a function of the ^{31}P chemical shift anisotropy, $\delta_{aniso} = (\delta_{zz} - \delta_{iso})$, and the asymmetry parameter, $\eta = (\delta_{yy} - \delta_{xx})/(\delta_{zz} - \delta_{iso})$. (The axially symmetric ^{31}P chemical shift tensor is characterized by $\eta = 0$; increase in the contribution of the rhombic component is accompanied by increasing η in the 0–1 range.) The value $\eta = 0.31 \pm 0.03$ obtained for **I** reflects the predominantly axial symmetry of the ^{31}P chemical shift tensor but with a noticeable increase in the rhombicity. The orientation of the ^{31}P CP/MAS NMR spectra corresponds to δ_{xx} (59.5 ± 0.8 ppm) < δ_{yy} (76.1 ± 0.8 ppm) < δ_{zz} (149.3 ± 0.2 ppm) with positive δ_{aniso} = 54.3 ± 0.2 ppm. The ^{31}P CP/MAS NMR spectral measurements performed earlier for various transition and post-transition metal dithiophosphates [27–33] demonstrated that positive δ_{aniso} values ($\delta_{zz} > \delta_{iso}$) characterize the Dtph groups with the bidentate terminal structural function, whereas negative values attest to either

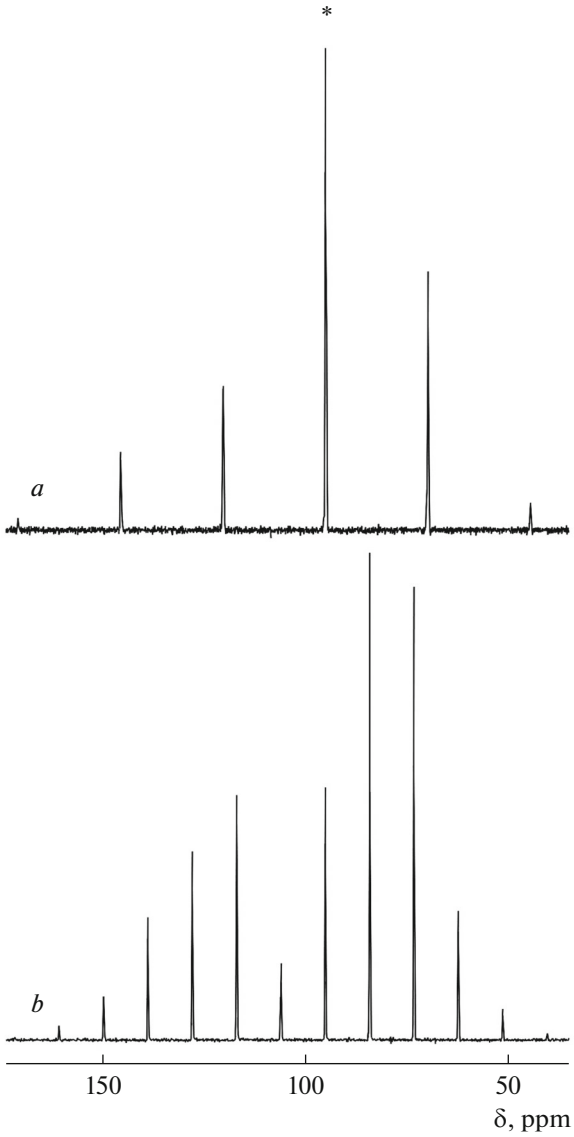

Fig. 2. ^{31}P MAS NMR spectra of compound **I**; number of acquisitions/spinning frequency: (*a*) 4/3.7 kHz, (*b*) 4/1.6 kHz.

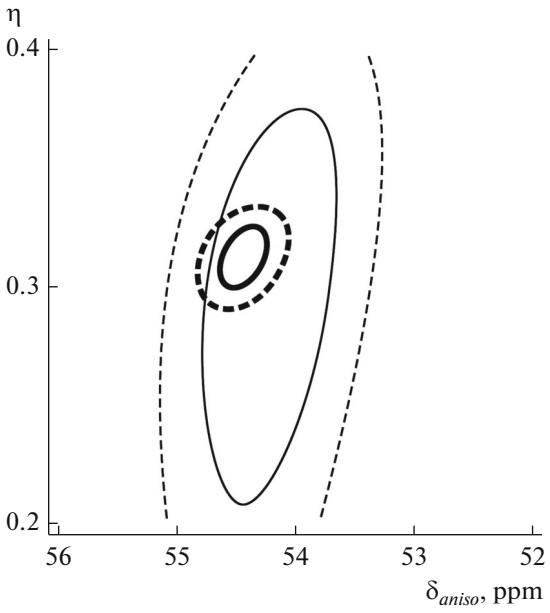

Fig. 3. χ^2-Statistic diagrams (for χ^2_{min}) as functions of ^{31}P chemical shift tensor anisotropy parameters for [Ni{$S_2P(O\text{-}i\text{-}C_5H_{11})_2$}$_2$]. Sample spinning frequencies: 1.6 kHz (thick lines) and 3.7 kHz (thin lines). Continuous lines circumscribe the areas of δ_{aniso} and η values for a confidence probability of 68.3%, dashed lines show the same for a confidence probability of 95.4%.

bridging or mixed (terminal bridging) function. The value $\delta_{aniso} = 54.3 \pm 0.2$ ppm obtained for nickel(II) di-*i*-amyl dithiophosphate attests to a bidentate terminal function of the Dtph ligands. Thus, according to ^{13}C and ^{31}P CP/MAS NMR data, compound **I** forms a highly symmetric molecular species incorporating equivalent Dtph ligands with a bidentate terminal function.

The unit cell of **I** comprises six structurally equivalent centrosymmetric [Ni{$S_2P(O\text{-}i\text{-}C_5H_{11})_2$}$_2$] molecules characterized by *S*,*S*'-isobidentate coordination of two Dtph ligands by the complexing ion (Fig. 4, Table 2). In molecule **I**, each carbon, oxygen, and sulfur atom is randomly distributed between two structural positions with equal occupancies. However, the disorder does not affect nickel and phosphorus atoms. These circumstances attest to the presence in **I** of two [Ni{$S_2P(O\text{-}i\text{-}C_5H_{11})_2$}$_2$] molecules rotated, relative to each other, around the P–Ni–P bisecting axis (which passes through both four-membered [NiS_2P] rings) and populating crystal lattice sites with equal probabilities (Fig. 5). The rotation angle between the [NiS_4] chromophore planes is 21.0(1)°. (The averaging of the carbon sites reflected in the experimental ^{13}C CP/MAS NMR spectrum at room temperature (Fig. 1) can be attributed to the fast vibration dynamics of the molecules around the P–Ni–P axis.)

The bidentate coordination of the Dtph ligands gives rise to two small-size four-membered [NiS_2P] metallacycles, which share a nickel atom to form the bicyclic [PS_2NiS_2P] system. The metallacycles have rather short non-valence Ni–P contacts (2.811 Å). The markedly longer distances between the opposing sulfur atoms (3.020 Å) determine the long axis of the rhombic distortion of the metallacycles. This configuration enables the *trans*-annular interaction between the nickel and phosphorus atoms (that is, through the space of small-size four-membered metallacycles rather than through a system of chemical bonds). Because of the high symmetry of the complex (*mmm* point group), the torsion angles in the metallacycles are 0° or 180°, indicating that the atoms composing them are coplanar. The diagonal SNiS angles equal to 180° also attest to a planar geometry of the tetragonal

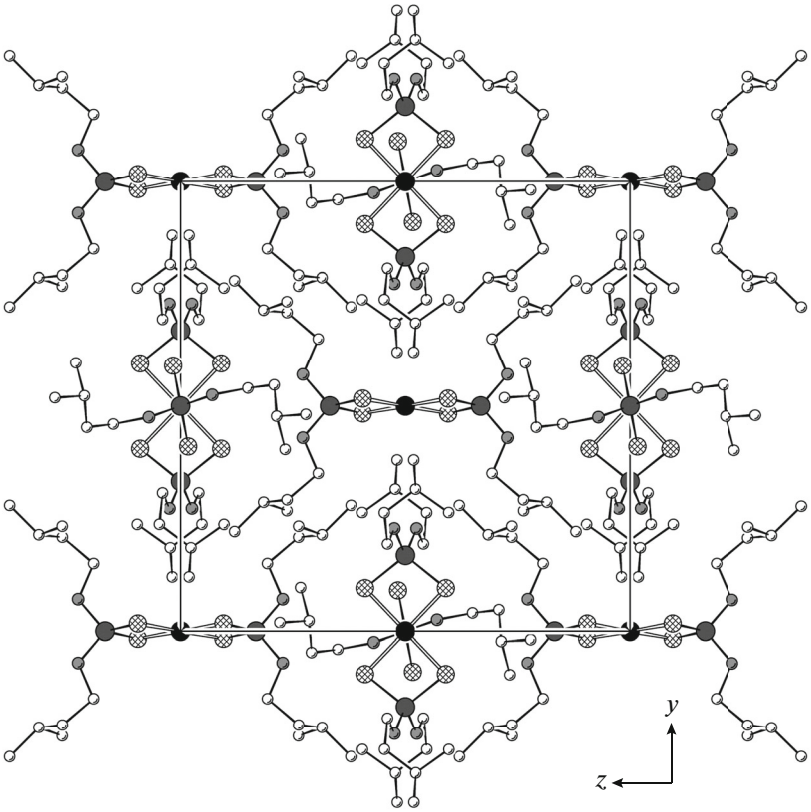

Fig. 4. Projection of the structure of $[Ni\{S_2P(O\text{-}i\text{-}C_5H_{11})_2\}_2]$ onto the *yz* plane.

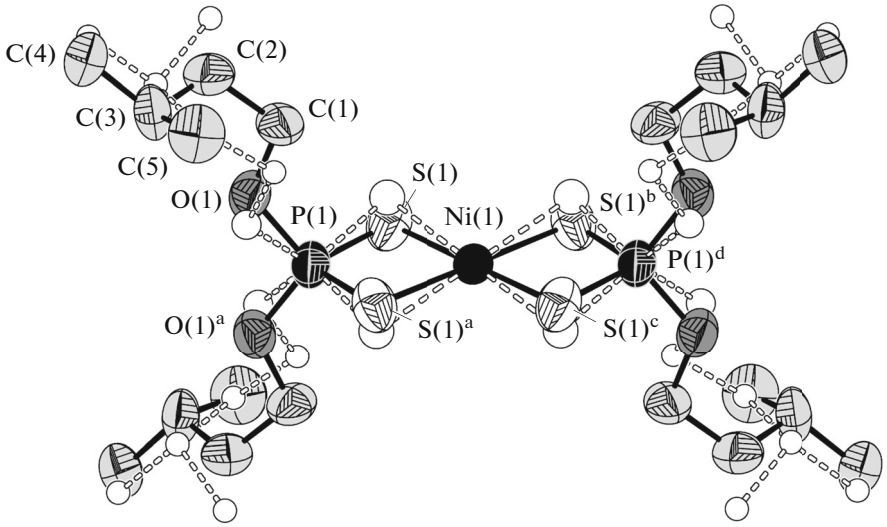

Fig. 5. Molecular structure of complex **I** with 30% probability ellipsoids. The hydrogen atoms are omitted. The alternative positions of the disordered atoms are shown by circles and bonds between them are depicted by dashed lines. Symmetry codes: [a] $1 - x, y, -z$; [b] $x, 1 - y, z$; [c] $1 - x, 1 - y, -z$; [d] $1 - x, 1 - y, z$.

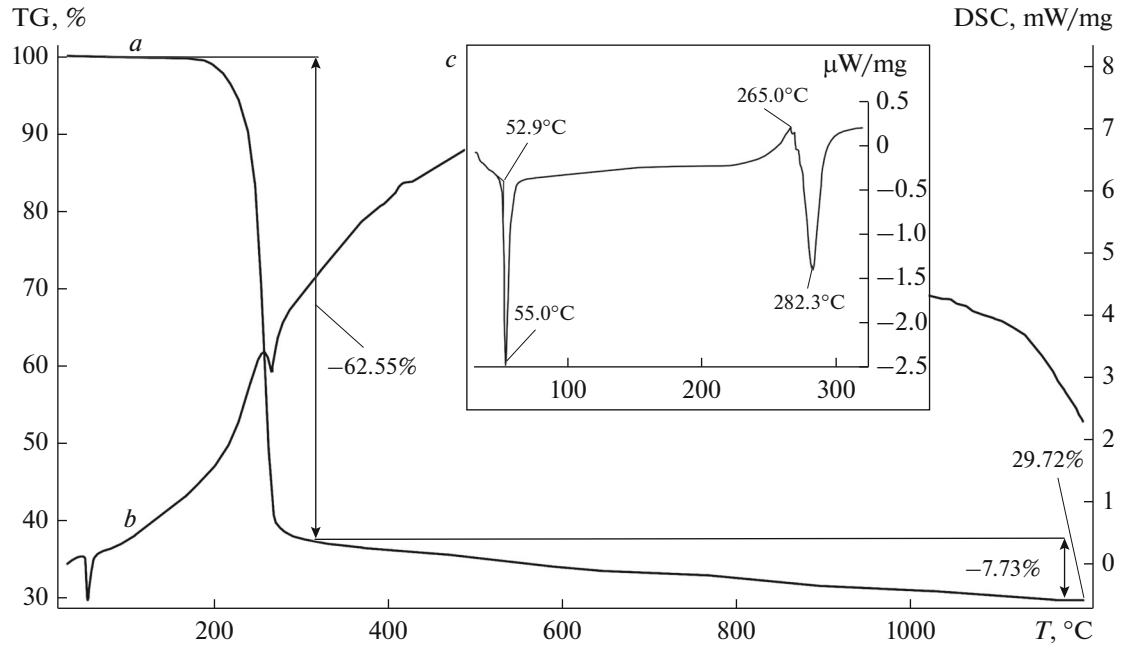

Fig. 6. (*a*) TG and (*b*, *c*) DSC curves for complex **I** (*c* is the low-temperature part of the DSC curves recorded in an aluminum crucible).

$[NiS_4]$ chromophores (intraorbital dsp^2 hybrid state of Ni atoms); and the S···S···S angles are 90°. The distortion of the tetrahedral $[O_2S_2]$ environment of phosphorus is caused by considerable deviation of the SPS, SPO, and OPO angles from 109.5° and by difference between the P–S and P–O bond lengths (Table 2). The averaging of the P–S bond length (1.960 Å), which is intermediate between the ideal single (2.14 Å) and double (1.94 Å) phosphorus–sulfur bond lengths [34] attests to π–electron density delocalization in the PS_2 groups.

The thermal behavior of nickel(II) di-*i*-amyl dithiophosphate was studied by STA under argon with simultaneous recording of TG and DSC curves. The TG curve (Fig. 6, *a*) shows the predominant weight loss (62.55%) related to the thermolysis of **I** in the steeply descending part of the curve (165–300°C). The highest weight loss rate occurs at 260.2°C. Then (300–1100°C) the TG curve arrives at a gently sloping part related to desorption of the thermal destruction products (7.73%). (It can be seen that even at 1100°C, the weight of the residue has not yet been stabilized.) The residue weight (29.72%) exceeds substantially the calculated weight (24.38%) of nickel(II) pyrophosphate, $Ni_2P_2O_7$ (m.p. = 1395°C [35]). However, apart from the yellow microcrystalline powder on the bottom (Fig. 7a), the crucible opened after completion of the process contained a dark gray deposit on the inner walls and on the lid, being due to formation of elemental carbon during the thermolysis in an argon atmosphere.

The DSC curve has two endotherms (Fig. 6, *b*). The first one, detected in the low-temperature region before the weight loss, was caused by the sample melting (extrapolated m.p. = 52.9°C). (Melting of a sample of **I** in a glass capillary (53.5–54.0°C) supports this conclusion.) The second endotherm with a peak at 282.3°C is related to thermolysis of complex **I**. The use of aluminum crucible reveals the internal structure of the latter endotherm (Fig. 6, *c*), indicating a complex nature of the thermolysis.

The chemical composition of the final thermolysis product was qualitatively characterized using electron probe microanalysis, which confirmed the presence of nickel, phosphorus, and oxygen (Fig. 7c) and the absence of sulfur, as opposed to the initial complex (Fig. 7b). An IR spectroscopic investigation of the residue showed absorption bands (1204–550 cm^{-1} range) due to the intramolecular vibrations of the pyrophosphate ion $P_2O_7^{4-}$. The IR spectrum shows characteristic stretching modes for the PO_3 (ν_s, $\nu_{as}(PO_3)$ 1098, 1070, and 1043 cm^{-1}) and bridging P–O–P (ν_{as}(POP) 979 cm^{-1}, ν_s(POP) 742 cm^{-1}) groups and bending modes for the P=O groups (δ(PO) 605 and 550 cm^{-1}). The general IR spectral pattern and the set, intensity, and positions of absorption bands imply that nickel(II) pyrophosphate $Ni_2P_2O_7$ is the major product of thermolysis [36, 37].

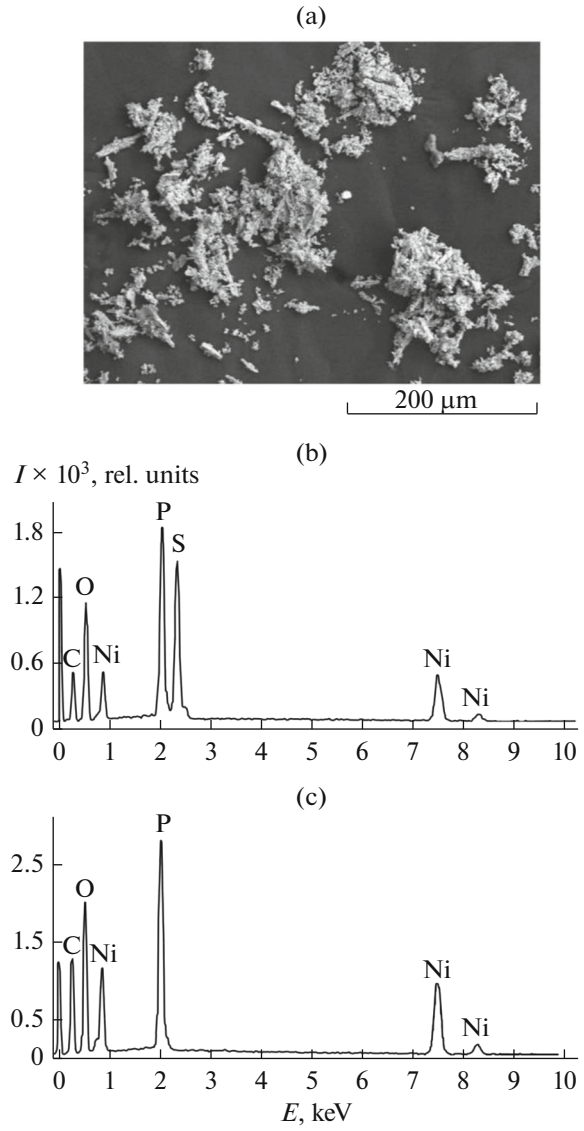

Fig. 7. (a) Particle size and shape for the final product of the thermal transformation of complex **I**; (b, c) energy dispersive spectra of the (b) polycrystalline [Ni{$S_2P(O\text{-}i\text{-}C_5H_{11})_2$}$_2$] and (c) the final residue after thermolysis at 1100°C.

ACKNOWLEDGMENTS

This work was partially supported by the Centre of Advanced Mining and Metallurgy, Sweden.

REFERENCES

1. Kastalsky, V. and McConnell, J.F., *Acta Crystallogr., Sect. B: Struct. Crystallogr. Cryst Chem.*, 1969, vol. 25, no. 5, p. 909.
2. Fernando, Q. and Green, C.D., *J. Inorg. Nucl. Chem.*, 1967, vol. 29, no. 3, p. 647.
3. McConnell, J.F. and Kastalsky, V., *Acta Crystallogr.*, 1967, vol. 22, no. 6, p. 853.
4. Paliwoda, D., Chojnacki, J., Mietlarek-Kropidlowska, A., and Becker, B., *Acta Crystallogr., Sect. E: Struct. Rep. Online*, 2009, vol. 65, no. 6, p. m662.
5. Ivanov, A.V., Larsson, A.-C., Rodionova, N.A., et al., Russ. *J. Inorg. Chem*. 2004, vol. 49, no. 3, p. 373.
6. Hoskins, B.F. and Tiekink, E.R.T., *Acta Crystallogr., Sect. C: Crystal Struct. Commun.*, 1985, vol. 41, no. 3, p. 322.
7. Bolundut, L., Haiduc, I., Ilyes, E., et al., *Inorg. Chim. Acta*, 2010, vol. 363, no. 15, p. 4319.
8. Taş, M., Yağan, M., Bati, H., et al., *Indian J. Chem.*, 2008, vol. 47, no. 1, p. 37.
9. Taş, M., Yağan, M., Bati, H., et al., *Acta Crystallogr., Sect. E: Struct. Rep. Online*, 2005, vol. 61, no. 9, p. m1684.
10. Lin, C., Liu, S., Xu, Z., et al., *Chin. J. Struct. Chem.*, 1987, no. 3, p. 186.
11. Bingham, A.L., Drake, J.E., Light, M.E., et al., *Polyhedron*, 2006, vol. 25, no. 4, p. 945.
12. Zou, L.K., Xie, B., Xie, J.Q., et al., *Transition Met. Chem.*, 2009, vol. 34, no. 4, p. 395.
13. Zhang, X.-L., Zou, L.-K., Xie, B., et al., *Chin. J. Struct. Chem.*, 2013, vol. 32, no. 5, p. 779.
14. Biscarini, P., Benedetti, M., Ferranti, F., et al., *Chirality*, 2004, vol. 16, no. 4, p. 251.
15. Ye, Q., Pang, J., and Qu, Z.-R., *Chin. J. Inorg. Chem.*, 2005, vol. 21, no. 10, p. 1589.
16. Lai, C., Xie, B., Zou, L.-K., and Feng, J.-S., *Acta Crystallogr., Sect. E: Struct. Rep. Online,* 2011, vol. 67, no. 1, p. m17.
17. Gianini, M., Caseri, W.R., Gramlich, V., and Suter, U.W., *Inorg. Chim. Acta*, 2000, vol. 299, no. 2, p. 199.
18. Pines, A., Gibby, M.G., and Waugh, J.S., *J. Chem. Phys.*, 1972, vol. 56, no. 4, p. 1776.
19. Earl, W.L. and Vanderhart, D.L., *J. Magn. Reson.*, 1982, vol. 48, no. 1, p. 35.
20. Morcombe, C.R. and Zilm, K.W., *J. Magn. Reson.,* 2003, vol. 162, no. 2, p. 479.
21. Karaghiosoff, K., in *Encyclopedia of Nuclear Magnetic Resonance*, Grant, D.M. and Harris, R.K., Eds., New York: Wiley, 1996, vol. 6, p. 3612.
22. Press, W.H., Teukolsky, S.A., Vetterling, W.T., and Flannery, B.P., *Numerical Recipes in C*, Cambridge: Cambridge Univ., 1994.
23. Hodgkinson, P. and Emsley, L., *J. Chem. Phys.*, 1997, vol. 107, no. 13, p. 4808.
24. Antzutkin, O.N., Lee, Y.K., and Levitt, M.H., *J. Magn. Reson.*, 1998, vol. 135, no. 1, p. 144.
25. Wolfram, S., *The Mathematica Book*, Cambridge: Wolfram Media/Cambridge Univ., 1999.
26. *APEX2 (version 1.08), SAINT (version 7.03), SADABS (version 2.11) and SHELXTL (version 6.12)*, Madison: Bruker AXS Inc., 2004.
27. Larsson, A.-C., Ivanov, A.V., Forsling, W., et al., *J. Am. Chem. Soc.,* 2005, vol. 127, no. 7, p. 2218.
28. Larsson, A.-C., Ivanov, A.V., Pike, K.J., et al., *J. Magn.* Reson., 2005, vol. 177, no. 1, p. 56.

29. Ivanov, A.V., Gerasimenko, A.V., Antzutkin, O.N., and Forsling, W., *Inorg. Chim. Acta*, 2005, vol. 358, no. 9, p. 2585.
30. Rodina, T.A., Ivanov, A.V., Lavrent'eva, S.I., et al., Russ. *J. Inorg. Chem.*, 2008, vol. 53, no. 7, p. 1098.
31. Rodina, T.A., Ivanov, A.V., Konfederatov, V.A., et al., Russ. *J. Inorg. Chem.*, 2009, vol. 54, no. 11, p. 1779.
32. Korneeva, E.V., Rodina, T.A., Ivanov, A.V., et al., Russ. *J. Coord. Chem.*, 2014, vol. 40, no. 10, p. 748.
33. Rodina, T.A., Korneeva, E.V., Antzutkin, O.N., and Ivanov, A.V., *Spectrochim. Acta, Part A*, 2015, vol. 149, p. 881.
34. Lawton, S.L. and Kokotailo, G.T., *Inorg. Chem.*, 1969, vol. 8, no. 11, p. 2410.
35. Lidin, R.A., Andreeva, L.L., and Molochko, V.A., *Spravochnik po neorganicheskoi khimii* (Handbook in Inorganic Chemistry), Moscow: Khimiya, 1987.
36. Nakamoto, K., *Infrared Spectra and Raman Spectra of Inorganic and Coordination Compounds*, New York: Wiley, 1986.
37. Onoda, H., Ohta, T., and Kojima, K., *Mater. Chem. Phys.*, 2006, vol. 98, nos. 2–3, p. 363.

Translated by Z. Svitanko